

Article

High-Precision Laboratory Dryer for Characterization of the Drying Behavior of Agricultural and Food Products

Sebastian Reyer ^{*}, Sebastian Awiszus  and Joachim Müller 

Institute of Agricultural Engineering, Tropics and Subtropics Group, University of Hohenheim, Garbenstraße 9, 70599 Stuttgart, Germany; sebastian.awiszus@uni-hohenheim.de (S.A.); joachim.mueller@uni-hohenheim.de (J.M.)

* Correspondence: info440e@uni-hohenheim.de

Abstract: To reduce the energy consumption during the drying of agricultural and food products, the optimization of the drying process with regard to the drying behavior and the quality of the end products is necessary. Therefore, much effort is spent designing and developing dryers to study the drying behavior of a wide range of products. This often results in a trade-off between measurement accuracy and the sufficient production of dried material required for the product quality analysis. Therefore, a laboratory dryer was developed consisting of three high-precision drying columns, each able to process 600 g of sample mass, and a flatbed dryer that can be loaded with 20 kg of fresh product. Drying curves could be recorded simultaneously by electronic balances in the three precision dryers and the flatbed dryer. The high-precision laboratory dryer HPD TF3+ proved to be suitable for establishing drying curves for a defined temperature, rel. humidity and velocity of the drying air.

Keywords: postharvest technology; precision drying; sorption isotherms; drying behavior; thin-layer dryer; flatbed dryer; HPD TF3+



Citation: Reyer, S.; Awiszus, S.; Müller, J. High-Precision Laboratory Dryer for Characterization of the Drying Behavior of Agricultural and Food Products. *Machines* **2022**, *10*, 372. <https://doi.org/10.3390/machines10050372>

Academic Editor: Angelos P. Markopoulos

Received: 26 March 2022

Accepted: 11 May 2022

Published: 13 May 2022

Publisher's Note: MDPI stays neutral with regard to jurisdictional claims in published maps and institutional affiliations.



Copyright: © 2022 by the authors. Licensee MDPI, Basel, Switzerland. This article is an open access article distributed under the terms and conditions of the Creative Commons Attribution (CC BY) license (<https://creativecommons.org/licenses/by/4.0/>).

1. Introduction

To minimize storage losses and to reduce transportation costs, the drying of agricultural commodities and food products is a well-established and commonly used method. During drying, water is removed from the product and, consequently, the water activity is decreased. Thus, the enzymatic processes and the microbiological activity are widely inhibited, resulting in a longer shelf life. The drying conditions must be selected in such a way as to retain the valuable ingredients [1,2]. However, the drying of food products is a process with a high energy demand [3]. To reduce the energy consumption during drying, the optimization of the drying process with regard to the drying time and the quality of the end products is necessary. Therefore, much effort has been spent at research institutions to design and develop laboratory dryers to study the drying behavior of a wide range of products.

In the literature, various laboratory dryers for agricultural commodities and food products have been described. The dryers are operated in different air-flow modes, such as over-flow [1,4,5], through-flow [6–8], cross-flow [9,10] and without forced convection (oven drying) [11–14], and the water evaporation is typically measured in terms of mass loss by means of a weighing device.

To ensure the best possible quality of the end products, it is necessary to know the permissible drying temperature and the optimum drying time. This is the only way to achieve a compromise between the most cost-efficient drying method and the best possible product quality. In order to investigate the effect of drying on the product quality, the dried products must be analyzed by standard laboratory methods depending on the type of ingredients to be preserved. Therefore, a certain amount of dried product is needed after the drying experiments to perform the required analyses. However, most laboratory dryers

with a high balance accuracy only allow a low sample mass [15,16]. Until now, to obtain the required mass of dried products for the quality analyses, drying experiments have had to be repeated many times. However, most agricultural products are seasonal and have a narrow harvesting window, ranging from a few days to a few weeks, depending on the product. Furthermore, drying under different conditions can require a wide range of drying times from a few hours to a few days. Performing all the needed drying trials within the limited harvesting window remains challenging. Currently, this problem is solved either by reducing the number of trials or by purchasing multiple laboratory dryers, which is costly.

The aim of this study was therefore to develop a drying system suitable for precisely measuring the drying behavior of thin product layers and also to provide a sufficient sample mass for subsequent quality analyses of the product.

The starting point for the development was the high-precision laboratory dryer HPD T1, previously developed by the authors, which allows the drying behavior of a single sample to be measured per test run [17].

The further development of the laboratory dryer consisted in the extension to three precision drying columns able to process 600 g of sample mass each and the integration of a flatbed dryer that can be loaded with 20 kg of fresh product for subsequent quality analysis. On the one hand, this allows the monitoring of the drying kinetics of a thin product layer in three repetitions, and on the other hand, it allows the obtainment of a sufficient quantity of the dried product for quality analyses according to standard laboratory methods. Accordingly, HPD TF3+ was chosen as the acronym.

2. Materials and Methods

2.1. Design

The laboratory dryer is composed of five units: (1) the air-conditioning unit, which provides drying air of adjustable temperature and humidity; (2) the high-precision drying unit, which contains three drying columns, each with an axial fan providing an adjustable airflow; (3) the flatbed drying unit for drying larger sample masses for quality analyses; (4) the heat-loss compensation unit for maintaining stable temperature conditions; and (5) the balance unit for measuring the mass loss of the samples in the three drying columns. A schematic and a 3D model are shown in Figures 1 and 2, respectively, and the legend for both representations can be found in Table 1. The full set of 3D CAD data is available—for details, see Appendix A (Table A1) and Appendix B (Table A2).

2.1.1. Air-Conditioning Unit

A commercial climate chamber (type C 10/1000, CTS Clima Temperatur Systeme GmbH, Hechingen, Germany) was used to provide conditioned drying air in a range of $T = 10\text{--}90\text{ }^{\circ}\text{C}$, $\text{RH} = 10\text{--}95\%$ and with a dew-point temperature of $T_{\text{dew}} = -7\text{--}89\text{ }^{\circ}\text{C}$. To achieve a low T_{dew} , the climate chamber was equipped with an adsorption dryer. A specially installed outlet and inlet opening on the side connects the climate chamber to the dryer unit and circulates the conditioned air throughout the entire system. The climate chamber is controlled by the actual value measured by a T and RH sensor (type HC2-IC402/CTS, Rotronic Messgeräte GmbH, Ettlingen, Germany) (3.1) that is placed between the precision drying unit and the flatbed drying unit to maintain setpoint conditions. The accuracy is given for humidity with $\pm 0.8\%$ RH at $10\text{--}30\text{ }^{\circ}\text{C}$ and for temperature with $\pm 0.1\text{ }^{\circ}\text{C}$ at $10\text{--}30\text{ }^{\circ}\text{C}$.

2.1.2. High-Precision Drying Unit

The high-precision drying unit comprises three identical drying columns with a vertical structure, starting at the bottom with an aerodynamically shaped radial air inlet (2.1), followed by an axial fan (type 4412/2HHP, ebm-papst Muldingen GmbH und Co. KG, Muflingen, Germany) (2.2), a vane anemometer (type 00.14680.020400, Lambrecht Meteo GmbH, Göttingen, Germany) (2.3) and a steel mesh sample tray (2.4) on top that is connected by nylon strings (2.5) to the balance unit (5). The speed of the axial fans

is controlled to achieve the set air velocity in the drying columns, as measured by the vane anemometers.

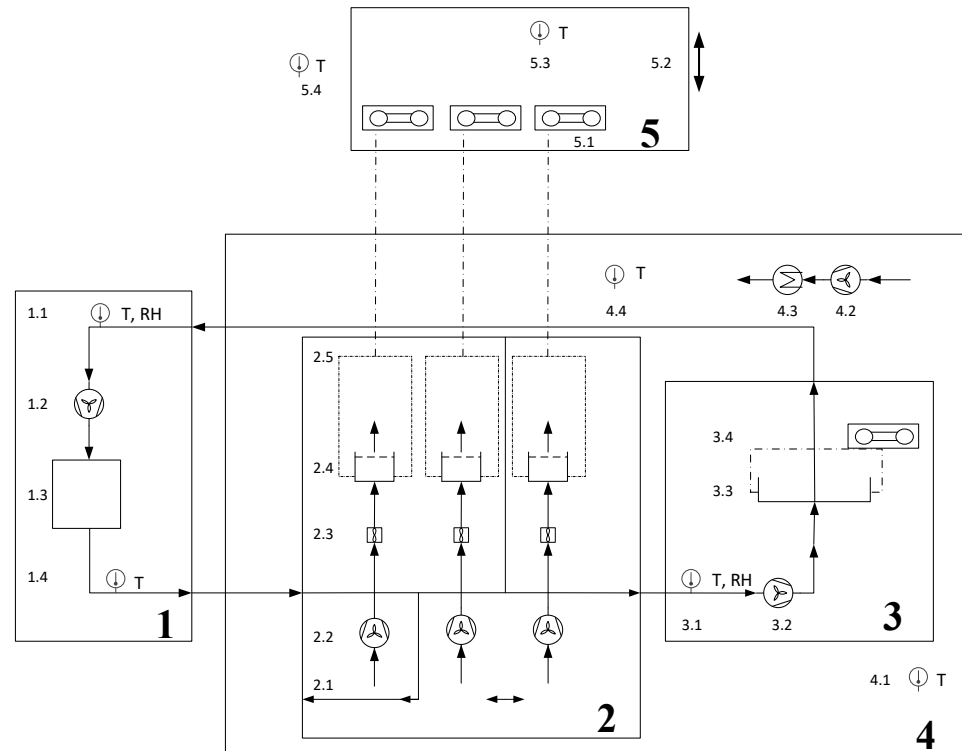


Figure 1. Schematic of the high-precision laboratory dryer HPD TP3+ (for legend, see Table 1).

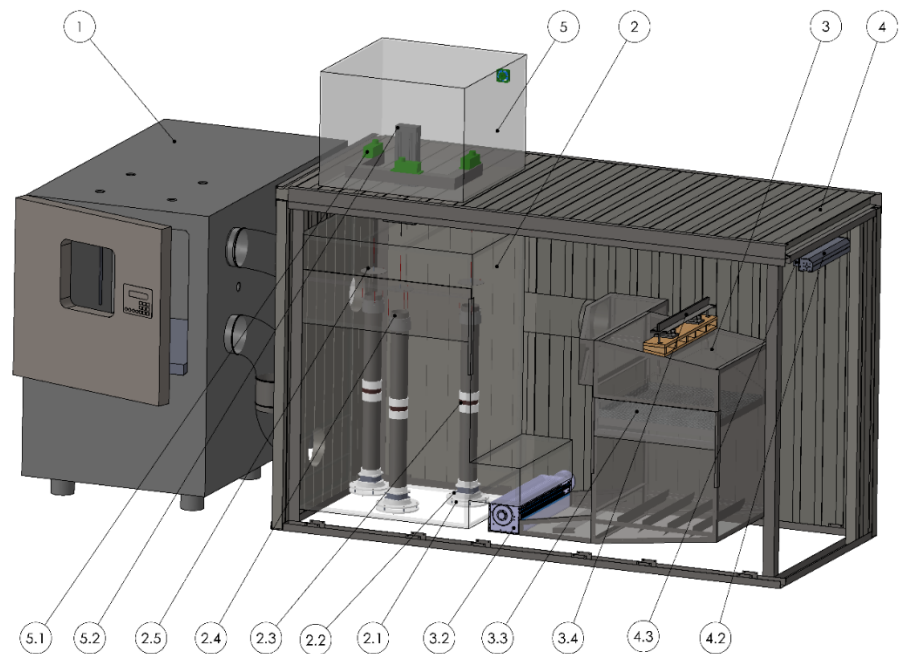


Figure 2. 3D model of the high-precision laboratory dryer HPD TP3+; 3D image with numbered subsystems (for legend, see Table 2).

Table 1. Legend for the high-precision laboratory dryer HPD TP3+ in Figures 1 and 2.

	Description
1	Air-conditioning unit
1.1	T and RH sensor
1.2	Controllable fan
1.3	Air conditioning inside the climate chamber
2	High-precision drying unit
2.1	Radial air inlet of drying column
2.2	Axial fan
2.3	Vane anemometer
2.4	Sample tray with through flow
2.5	Traverse with nylon strings
3	Area drying unit
3.1	T and RH sensor
3.2	Cross-flow fan
3.3	Sample tray with through flow
3.4	Traverse with bending beam load cells
4	Heat-loss compensation unit
4.1	T sensor
4.2	Cross-flow fan
4.3	Electrical heater
4.4	T sensor
5	Balance unit
5.1	High-precision load cells
5.2	Linear lifting unit
5.3	T sensor
5.4	T sensor, ambient

Table 2. Air velocity (v_{meas}) in drying column with empty sample trays at different v_{set} in the HPD TF3+; min, max and MAPE values after a start-up phase of 50 s.

v_{set} $\text{m}\cdot\text{s}^{-1}$	v_{min} $\text{m}\cdot\text{s}^{-1}$	v_{max} $\text{m}\cdot\text{s}^{-1}$	MAPE (v) %
0.2	0.09	0.34	7.46
0.4	0.24	0.58	4.92
0.6	0.43	0.78	3.91
0.8	0.51	0.99	3.07
1.0	0.80	1.23	2.29
1.2	0.92	1.44	2.08

The columns were filled with a honeycomb material to obtain a uniform airflow. Nylon strings were used instead of steel wires to suspend the sample trays, as they have lower thermal conductivity and thus provide better protection against the condensation of water at the transition to the balance unit.

2.1.3. Balance Unit

For the weighing of the sample trays in the high-precision drying unit, three electronic balances (5.1) (type WZA1203-N, Sartorius AG, Göttingen, Germany) with a capacity of $1200\text{ g} \pm 0.001\text{ g}$ are mounted on a traverse that is attached to a linear lifting unit (5.2) (type LES 6 L = 490 mm, Isel Germany AG, Eichenzell, Germany). The lifting unit is mounted on the top of the high-precision dryer outside the heat-loss compensation unit. To decouple the balance unit from the varying ambient temperature, an insulated box is placed around the balance unit. To weigh the sample trays within a set time interval, the traverse is lifted until the trays hang freely. Matching cones on the bottom of the sample trays and the top of the drying columns ensure an airtight upright position when the sample tray is set back

after weighing. During weighing, all fans throughout the entire system are stopped to avoid vibrations.

2.1.4. Flatbed Drying Unit

The flatbed dryer has an area of 800 mm × 800 mm divided into two removable trays made of perforated steel plate. The trays are placed on a frame suspended from a traverse that is attached to two bending beam load cells (3.4) (type MP77/20 kg C3MR, Minebea Intec GmbH, Hamburg, Germany) for mass measurement, with a total capacity of 40 kg ± 0.02%. A tangential fan (3.2) (type TMR 125/800/E, LTG AG, Stuttgart, Germany) conveys the air from the air-conditioning unit through the high-precision drying unit towards the flatbed drying unit, where air baffles guide the airflow through the trays. After passing the product, the drying air is guided back towards the air-conditioning unit and readjusted for the next cycle. In contrast to the high-precision unit, the air velocity in the flatbed drying unit is variable and can be adjusted via potentiometer to a fixed value.

2.1.5. Heat-Loss Compensation Unit

Both the high-precision drying unit and the flatbed drying unit are made of stainless steel and must be tempered to the drying temperature. Therefore, they are placed in a thermally insulated housing made of sandwich elements that is heated with an integrated electrical heating element (4.3) (type TAR h 60/615/24VDC 3 kW, 230 V, LTG AG, Stuttgart, Germany) attached to an additional tangential fan (4.2) providing smooth air circulation without disturbing the weighing process. The system is controlled to compensate for the heat loss through the housing.

To allow access to the drying units for handling and observation, openings with sliding acrylic doors are provided at the front. For maintenance, the front and rear panels are designed to be easily removed.

2.2. Operation of the Laboratory Dryer

The operation parameters depend on the product properties. The airflow velocity of the high-precision drying unit can be adjusted from $v = 0.2$ to $1.5 \text{ m}\cdot\text{s}^{-1}$. The air condition parameters can be chosen within $T = 20\text{--}80 \text{ }^\circ\text{C}$ and $\text{RH} = 5\text{--}95\%$.

After starting the control program, which is shown schematically in Figure 3, the initialization and the preheating phase is executed automatically. Since the heating capacity of the air-conditioning unit is greater than its cooling capacity, the heat-loss compensation unit should be tempered at $\Delta T = 0.5\text{--}1 \text{ K}$ below the set drying temperature. The fans are activated to the set speed to create air circulation. When all T values are stable, the calibration process can be activated.

For the weighing process, all fans are stopped until the vane anemometers show zero velocity, and the sample trays are lifted in a freely suspended position. A break of 5 s is initiated to align the sample trays. When the mass values are stable, the values are recorded and the sample trays are lowered and reinserted into the positive fitting.

When the calibration is completed, the sample trays can be removed for loading via the sliding doors of the heat-loss compensation unit and the drying units. When more time is needed for sample preparation, the system automatically switches back to the preheating process step. When the samples are loaded and the drying process is started, the weighing cycle is performed in a set time interval. The measurement data are plotted for online observation of the drying process. The recorded data are also saved in a text file on the computer for storage and further processing. When the desired drying level is reached, the drying process is stopped, and the samples can be removed for further analyses.

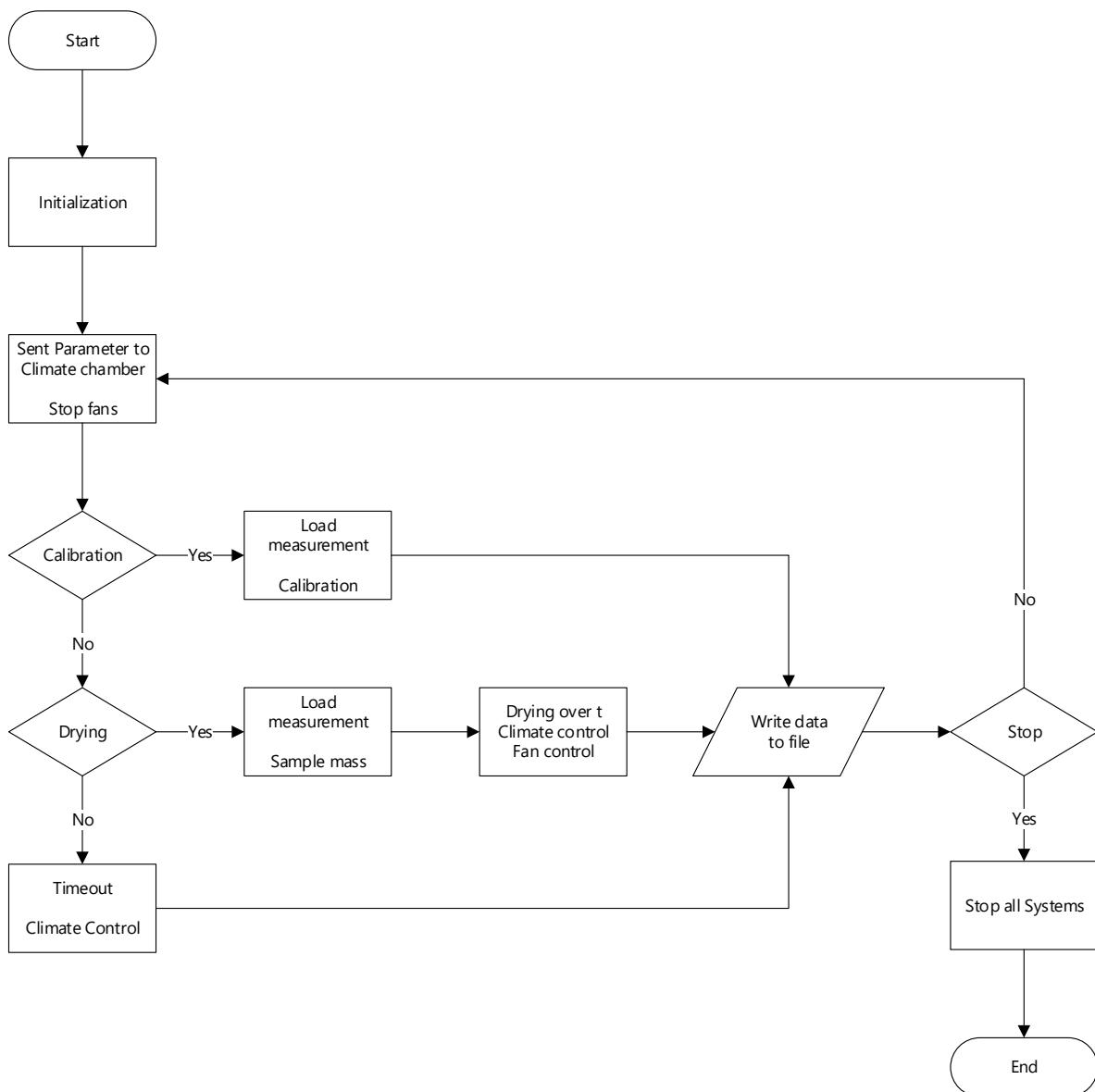


Figure 3. Schematic flowchart of HPD TP3+ control software.

3. Results

3.1. Calibration of Fan and Vane Anemometer

The vane anemometers were calibrated with a 50 mm diameter inlet nozzle mounted at the top of the dryer column according to VDI 2041 [18], and the vane anemometer and the fan were turned to force the airflow from top to bottom. The differential pressure was measured with a hand-held measuring device (type GDH 01 AN 0, . . . , 1999 Pa, Greisinger electronic, GHM Messtechnik GmbH, Regenstauf, Germany). The fan velocity was set up to a duty cycle from 10 to 100% in increments of 10%. When the fan reached a constant rotation speed, the pressure value and the voltage were recorded by the software for 5 s. Then, the next duty cycle step was started. The cycle was repeated three times for each vane anemometer. Finally, the average was calculated based on all measurements and installed vane anemometers.

The linear trend of the average velocity over voltage can be described by Equation (1) at $R^2 = 0.9997$ and a mean absolute percentage error (MAPE) of 1.0%.

$$v = 32.628 \cdot U + 0.1132 \quad (1)$$

where v is the air velocity in m s^{-1} , and U is the voltage in V .

Mean average percentage error (MAPE) was calculated as:

$$\text{MAPE} = \frac{100}{n} \sum_{t=1}^n \left| \frac{X_{\text{set}} - X_{\text{mea}}}{X_{\text{set}}} \right| \quad (2)$$

The characteristic curve of the axial fan of the high-precision units is plotted for different rotation speeds with a maximum of $n = 5000 \text{ min}^{-1}$ as the upper boundary condition in Figure 4. In addition, the resistance curve of the drying column with an empty sample tray is shown as the lower boundary. As the remaining boundary condition, the minimum detection velocity of the vane anemometer is plotted at $v = 0.2 \text{ m}\cdot\text{s}^{-1}$. The area within the three boundaries marks the field of operation of the HPD TF3+ in the high-precision drying unit.

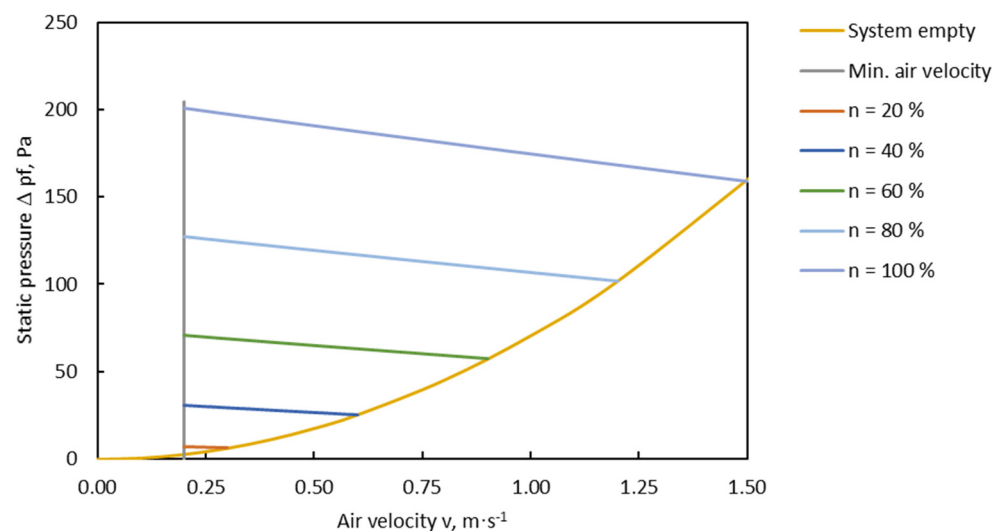


Figure 4. Static pressure Δp_f vs. air velocity v ; characteristic curves of fan type 4412/2 HHP for different rotation speeds n in % of maximal rotation speed, and airflow resistance curve of empty system.

The average air velocity of the three high-precision drying units for different set values is plotted in Figure 5. After a short start-up phase, the different set air velocities reached quite stable levels, as shown in Table 2 by the minimum, maximum and MAPE values recorded after a start-up phase of 50 s. A slow P-controller was chosen to prevent the overshooting of the set value, because rapid overdriving could result in a blowout of light particles from the sample trays.

3.2. Calibration of Electronic Balances

The electronic balances P1, P2 and P3 of the three drying columns of the high-precision drying unit and the load cells F of the flatbed dryer have to be calibrated before starting drying experiments. For calibrating the flatbed drying unit F, a dead load of $m_{\text{cal}} = 2999 \text{ g}$ was placed on the trays. To calibrate the high-precision balances, three dead loads of approximately 200 g were then placed on the trays of the drying columns. The accurate dead loads (m_{cal}) are shown in Table 3. The measured values over time are shown in Figures 6 and 7, together with the fluctuating ambient air in the technical building. The mass profiles in the high-precision unit were stable and smooth for mP1 and mP2. In contrast, mP3 showed slight vibrations that could have been caused by the airflow of the near tangential fan. The mass profile of the flatbed drying unit also showed a quite stable course. The fluctuations were caused by the low resolution of the converter. The measured minimum and maximum values and the MAPE are shown in Table 3. MAPE

values below 0.1% demonstrate the high precision of the balances even under fluctuating ambient temperatures between 14.5 and 20 °C.

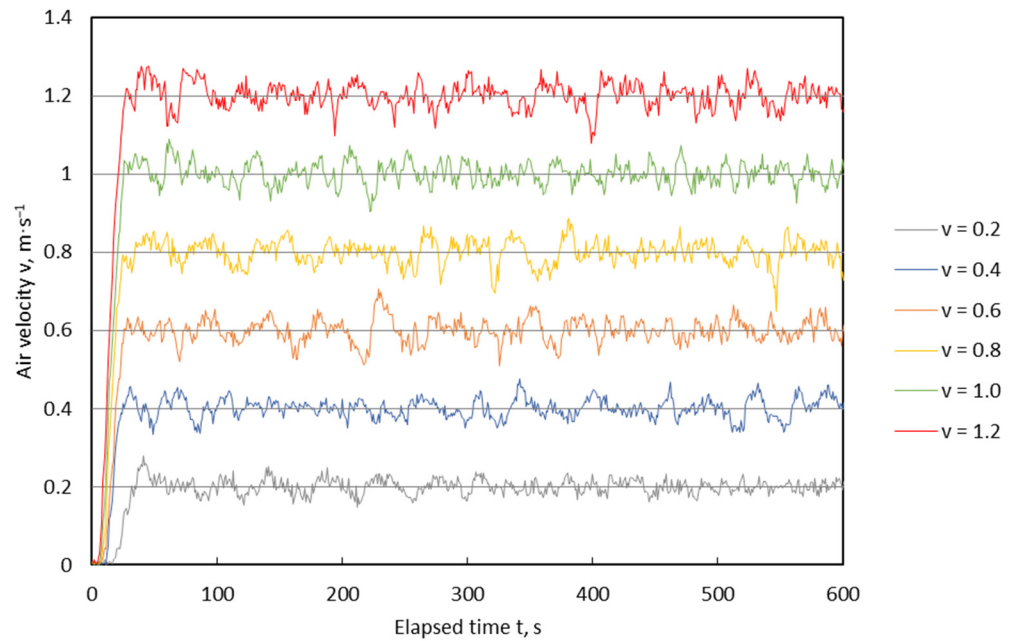


Figure 5. Air velocity vs. time; air velocity (v_{meas}) in the high-precision drying unit with empty sample trays at different v_{set} in the HPD TF3+ during calibration.

Table 3. Parameters during calibration of the electronic balances in the HPD TP3+.

Balance	T_{set} °C	RH_{set} %	m_{cal} g	m_{min} g	m_{max} g	MAPE (m) %
P1	30	33	204.21	204.18	204.30	0.01
P2	30	33	203.44	203.26	203.44	0.03
P3	30	33	200.94	200.67	201.36	0.03
F	30	33	2999	2976	3019	0.06

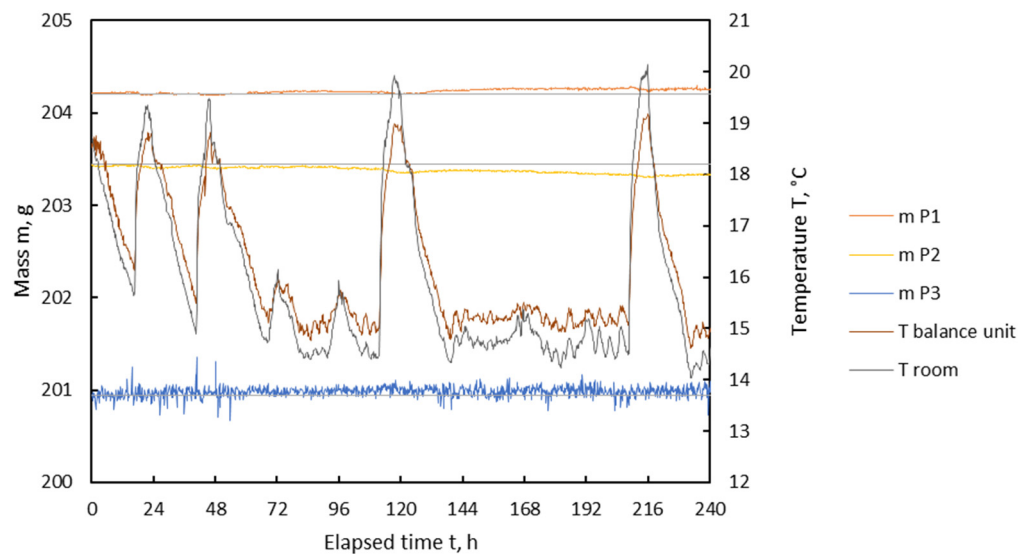


Figure 6. Temperature and mass vs. time; room temperature (T_{room}), temperature in balance unit ($T_{\text{balance unit}}$) and sample mass of precision drying zone (m_{P1} , m_{P2} , m_{P3}) in the HPD TF3+ during calibration.

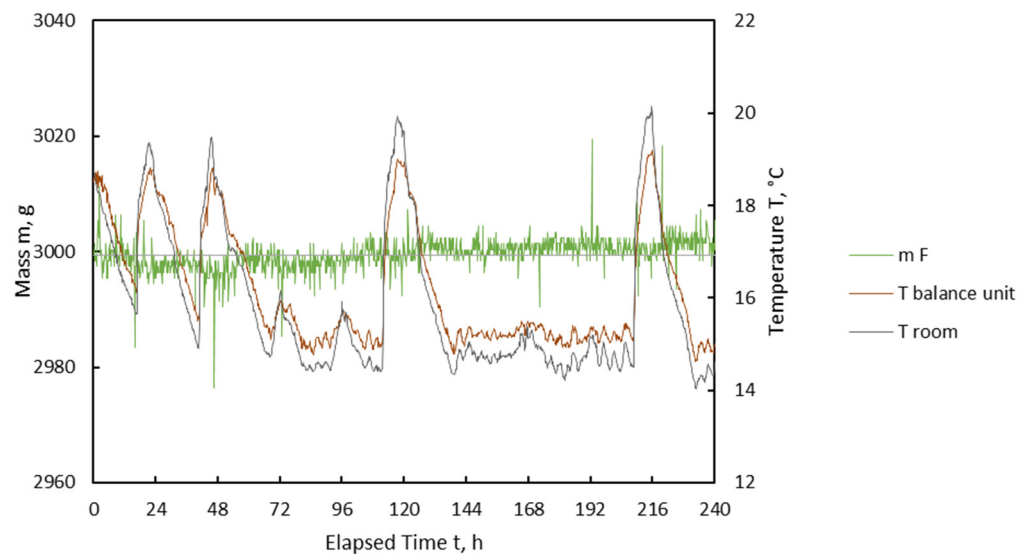


Figure 7. Room temperature and mass vs. time; room temperature (T_{room}) and sample mass of flatbed drying zone (m_F) in the HPD TF3+ during calibration.

3.3. Validation

For validation of the performance of the HPD TF3+, four test runs with nettles (*Urtica dioica* L.) at constant values of $x = 0.01$ and $v = 0.2 \text{ m}\cdot\text{s}^{-1}$ were performed for drying air temperatures (T) between 30 and 60 °C in steps of 10 K. The test runs showed a nearly constant course at the set temperature levels, as illustrated in Figure 8. Except for $T = 30 \text{ °C}$, the MAPE values were 0.81% or below, as shown in Table 4. For $T_{\text{set}} = 30 \text{ °C}$, the MAPE was higher, reaching 3.17%. This can be explained by the high ambient temperature that was temporarily above 30 °C. This meant that the air had to be cooled in the air-conditioning unit, where the cooling capacity was not always sufficient. Therefore, the ambient temperature should be below the drying temperature when using the system.

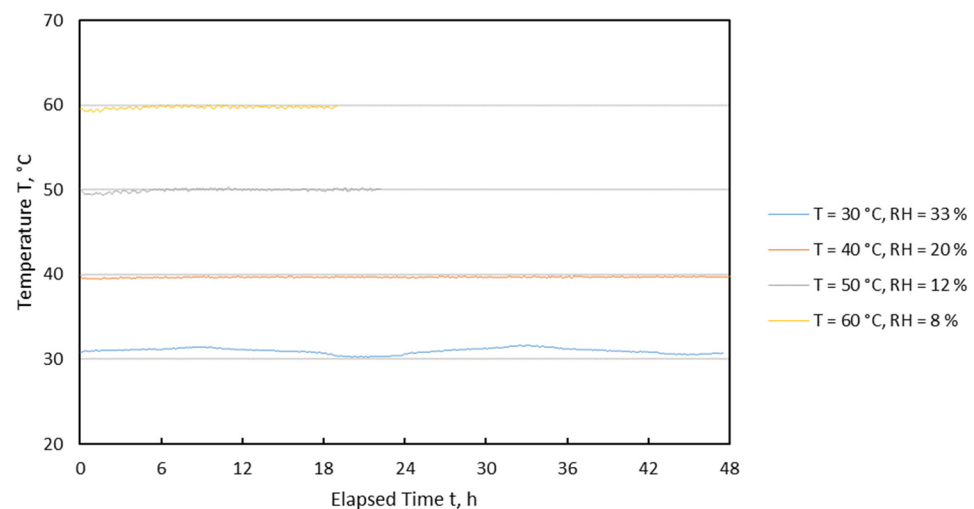
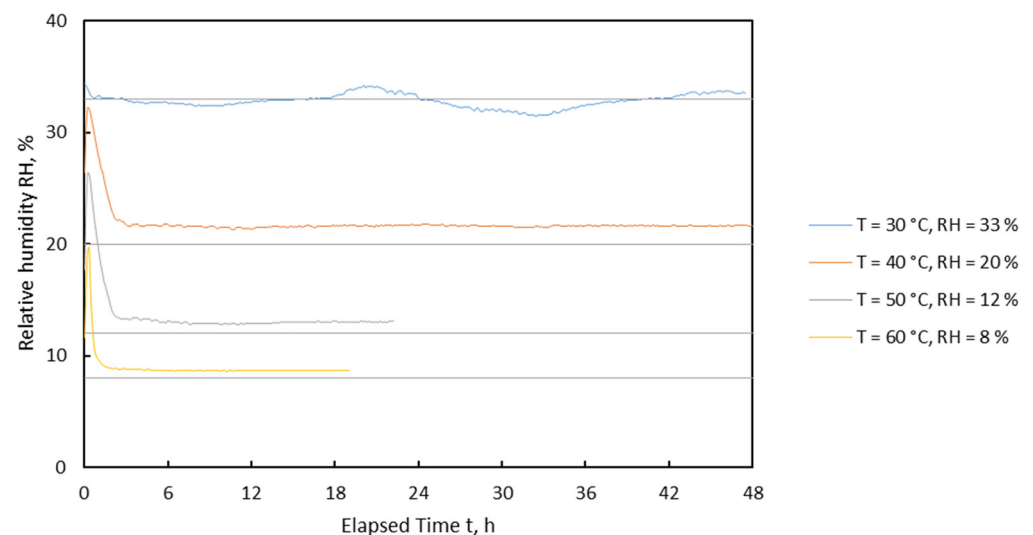


Figure 8. Temperature vs. time; temperature during drying of fresh nettles at different levels of set air temperature (T_{set}) in the HPD TP3+; $x_{\text{set}} = 0.01$, $v_{\text{set}} = 0.2 \text{ m}\cdot\text{s}^{-1}$.

Table 4. Parameters during drying of fresh nettles at different temperatures in the HPD TP3+.

T_{set} °C	RH_{set} %	T_{min} °C	T_{max} °C	RH_{min} %	RH_{max} %	x_{min} -	x_{max} -	MAPE (T) %	MAPE (RH) %	MAPE (x) %
30	33	30.2	31.6	31.5	34.3	0.009	0.010	3.17	1.51	5.06
40	20	38.4	40.0	21.0	32.2	0.010	0.015	0.81	9.33	2.40
50	12	49.4	50.3	12.8	26.4	0.010	0.021	0.26	13.44	8.33
60	8	59.2	60.0	8.6	19.7	0.011	0.025	0.42	12.45	14.71

Figure 9 shows the relative humidity of the drying air measured during the test runs at the different set temperatures. With the air at a constant water content (x), a higher temperature results in a lower relative humidity. The RH profile reached the set value in all test runs within a short time and remained stable in most cases. Only for $T = 30$ °C and $RH = 33\%$ did slight variations occur, which were caused by the temperature fluctuations explained above.

**Figure 9.** Relative humidity vs. time; relative humidity during drying of fresh nettles at different levels of set air temperature (T_{set}) in the HPD TP3+; $x_{\text{set}} = 0.01$, $v_{\text{set}} = 0.2 \text{ m}\cdot\text{s}^{-1}$.

Based on the measured T and RH , the actual water content (x_{calc}) of the drying air was calculated based on Equation (3):

$$x_{\text{calc}} = 0.622 \cdot \frac{\frac{RH_{\text{meas}}}{100} \cdot P_{w,\text{sat}}}{P - \frac{RH_{\text{meas}}}{100} \cdot P_{w,\text{sat}}} \quad (3)$$

where P is the barometric pressure and $P_{w,\text{sat}}$ is the water vapor saturation pressure at air temperature (T).

Figure 10 shows the x_{calc} of the drying air during the test runs at the different temperatures. All curves were expected to approach the set value of $x = 0.01$, which was largely the case after an initial adjustment phase. The deviation at $T = 60$ °C might be explained by the increasing inaccuracy of the RH sensor at high temperatures.

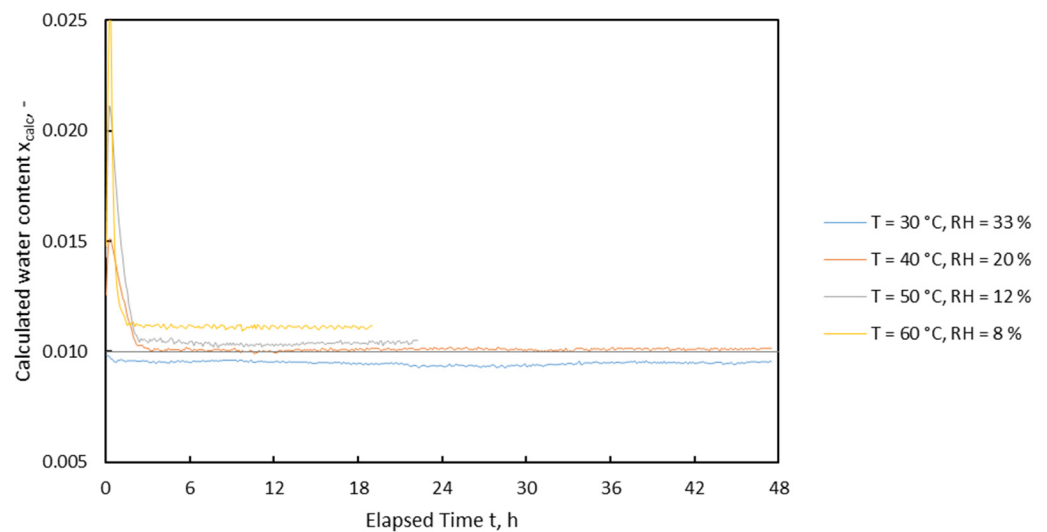


Figure 10. Calculated water content vs. time; calculated water content of air during drying of fresh nettles with different temperatures in the HPD TP3+; $x_{\text{set}} = 0.01$, $v_{\text{set}} = 0.2 \text{ m}\cdot\text{s}^{-1}$.

For validation of the weighing process during drying, the mass of the nettle samples was normalized as the mass ratio (MR):

$$\text{MR} = \frac{m_t}{m_0} \quad (4)$$

where m_t is the instantaneous mass at time t and m_0 is the initial mass at the start of the experiment.

In Figure 11, the mass ratio is exemplarily shown for the three drying columns and the flatbed dryer. The three high-precision dryers showed an almost identical course. The flatbed dryer deviated only slightly from the course, although the flatbed dryer was not designed to generate drying curves.

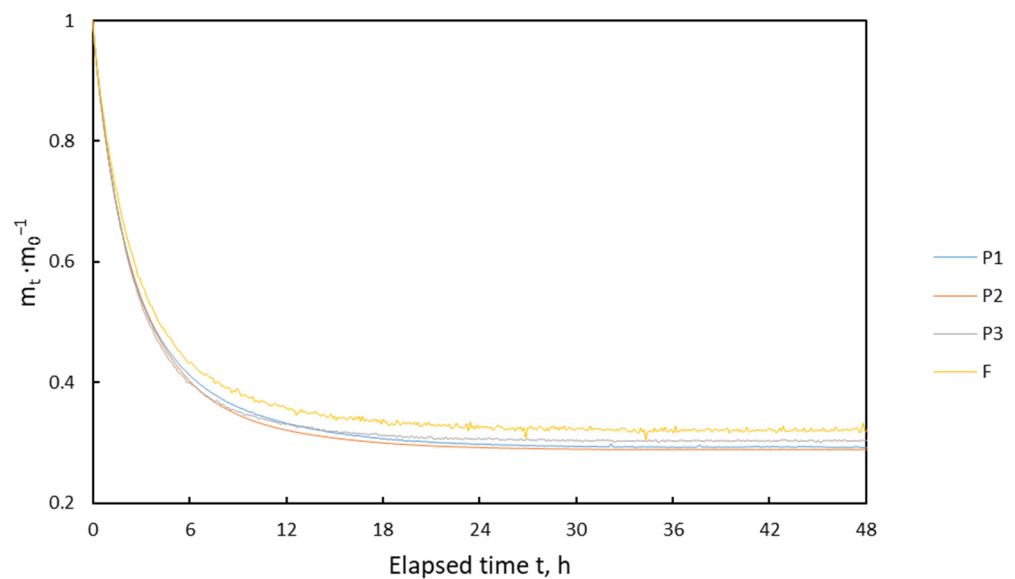


Figure 11. Mass ratio vs. time; normalized sample masses during drying of fresh nettles in the HPD TP3+; $T_{\text{set}} = 40 \text{ }^\circ\text{C}$, $\text{RH}_{\text{set}} = 20\%$, $v_{\text{set}} = 0.2 \text{ m}\cdot\text{s}^{-1}$.

4. Discussion

In the literature, various laboratory dryers have been described for conducting thin-film drying experiments with different operating conditions in terms of temperature,

relative humidity and the velocity of airflow, as well as the method and accuracy of measuring the mass of evaporated water. However, upon closer examination, there were always shortcomings of various kinds that justified the development of the high-precision laboratory dryer HPD TF3+. For example, Ajibola [12] described a laboratory dryer with a large range of air condition parameters, such as a temperature a range of -20 – 90 °C and relative humidity in the range of 0–100%. Additionally, the reading accuracy of the balance with ± 0.01 g at a total mass of 2100 g for each sample was high. For mass determination, however, the drying process had to be interrupted in order to weigh the sample manually on the balance. A continuous process was therefore not possible. Goyal et al. [10] presented a laboratory dryer with a continuous weighing system, allowing the establishment of accurate drying curves. The reading accuracy of the balance was ± 0.01 g, and temperature range was 30–110 °C. However, there was no provision for setting the relative humidity and the air velocity. In a laboratory dryer used by Ghnimi et al. [6], similar air conditions could be set as in the HPD TF3+. However, the airflow was from top to bottom, which can lead to the compaction of the drying material and thus to a distortion of the results. Furthermore, Duc et al. [19] used a laboratory dryer with a similar range of air conditions as in the HPD TF3+ and with a very precise weighing unit with an accuracy of ± 0.001 g. However, the maximum sample load was 4000 g, and successive repetitions were necessary for statistical analysis and to gain enough material for quality analyses. A larger sample mass of 20 kg was possible in a laboratory dryer described by Doymaz et al. [20]. However, the dryer was designed as a drying oven without the active ventilation of air. Therefore, the results could not be transferred to convective drying, which is most common in practice. Comparison with the literature shows that the laboratory dryer HPD TF3+ can avoid the various disadvantages of previously known laboratory dryers.

5. Conclusions

With the development of the laboratory dryer HPD TF3+, thin-layer drying experiments can be performed at a temperature range of 20 – 80 °C ± 0.1 °C, a relative humidity of 5 – $95\% \pm 0.8\%$ and an air velocity of 0.2 – 1.5 m·s⁻¹. Three samples of 600 g each can be dried simultaneously on high-precision balances of 1200 g ± 1 mg. Additionally, 20 kg of fresh product can be dried in the same airflow on a flatbed drying unit for analyzing the quality of the material after drying according to standard laboratory methods. The air conditions and the air velocity are controlled during the drying process and showed a high temporal stability.

The CAD files, software and a list of the parts of all relevant electrical components are provided to ensure that the system can be reproduced. In further research, the high-precision laboratory dryer will be used to investigate the drying kinetics of medicinal plants and the effect of drying conditions on the product quality.

Author Contributions: Conceptualization, S.R.; methodology, S.R. and S.A.; software, S.R.; validation, S.R. and J.M.; formal analysis, S.R. and J.M.; investigation, S.R.; resources, S.R.; data curation, S.R. and S.A.; writing—original draft preparation, S.R.; writing—review and editing, S.A. and J.M.; visualization, S.R.; supervision, J.M.; project administration, S.A.; funding acquisition, J.M. All authors have read and agreed to the published version of the manuscript.

Funding: This research received no external funding.

Institutional Review Board Statement: Not applicable.

Informed Consent Statement: Not applicable.

Data Availability Statement: Not applicable.

Conflicts of Interest: The authors declare no conflict of interest.

Appendix A

Source File Repository

For replicating the machine, all necessary files can be found in the source file repository: <http://dx.doi.org/10.17632/vg7c8dh365.1> (accessed on 10 November 2021).

1. HPD TF3+.EASM Assembly file for gaining an overview of the construction and operation. eDrawings is a free 3D viewer of 3DS: <https://www.edrawingsviewer.com/download-edrawings> (accessed on 10 November 2021).
2. HPD TF3+_FullSW.zip SolidWorks files with all the components for reproduction or improvements;
3. HPD TF3+.IGS IGS files with all the components for reproduction or improvements;
4. 2021_HPDTF3+_Electrical.pdf Electrical circuits for the balance heating unit and the PWM control;
5. HPD TF3+ Install.zip Contains the installer for the control program and the LabView runtime engine for Microsoft Windows.

Table A1. Design files.

Design File Name	File Type	Open Source License
HPD TF3+_FullSW.zip	zip//SolidWorks parts and assembly files	CC BY 4.0
HPD TF3+.IGS	igs	CC BY 4.0
HPD TF3+.EASM	easm	CC BY 4.0
2021_HPDTF3+_Electrical.pdf	pdf	CC BY 4.0
HPD TF3+ Install.zip	zip	CC BY 4.0

Appendix B

Table A2. Summary of materials bill.

	#	Company	Location	Country	Type	Price/pcs (EUR)	Total (EUR)
Climate chamber	1	CTS Clima Temperatur Systeme GmbH	Hechingen	D	C 10/1000	42,786.45	42,786.45
Axial fan	2.2	ebm-papst Mulfingen GmbH & Co. KG	Mulfingen	D	Fan 4412/2HHP	58.67	176.00
Vane anemometer	2.3	LAMBRECHT meteo GmbH	Göttingen	D	00.14680.020400 (1468)	1432.56	4297.67
Balance	5.1	Sartorius AG	Göttingen	D	WZA1203-N	3558.10	10,674.30
Linear lifting unit	5.2	isel Germany AG	Eichenzell	D	LES 6	1768.86	1768.86
Balance	3.4	Minebea Intec GmbH	Hamburg	D	2 × MP77/20 kg C3MR + 2 × MP97/00 N + MP 90/04+ MP 30/00 + MP 30/31, PR 1256/31	3105.90	3105.90
Control technology		National Instruments Germany GmbH	München	D	NI cDAQ-9184, NI9215, NI9217, NI9401, NI9263	4394.02	4394.02
Converter		IC Intracom Vertriebs GmbH	Halver	D	PCI-RS232 Card Part No.: 158213	17.99	53.97
Control pc				D	PC with Windows 10	700.00	700.00
Construction material		Esslinger Eisenlager GmbH	Esslingen	D	Steel	2528.77	2528.77
Vibration damper		EFFBE GmbH	Bad Soden-Salmünster	D	LM 480 daN	31.06	248.47

Table A2. Cont.

	#	Company	Location	Country	Type	Price/pcs (EUR)	Total (EUR)
Vent pipe		ERO Edelstahl-Rohrtechnik GmbH	Salzwedel	D	Vent pipe	501.55	501.55
Perforated plate		MEVACO GmbH	Göppingen	D	Perforated steel plate	196.59	196.59
Cross-flow fan	3.2	LTG Aktiengesellschaft	Stuttgart	D	TMR 125/800/E	2676.31	2676.31
T sensors	4.1, 4.4, 5.3, 5.4	TMH Elektrotechnik GmbH	Ellerbek	D	4* PT100	52.48	209.92
Electrical parts		Conrad		D	Electrical parts	750.00	750.00
Sandwich panel	4	Ranrode GmbH	Wettin-Löbejün	D	Isopanel RANWAND K 80 Typ IP	1022.93	1022.93
Cross-flow fan	4.2, 4.3	LTG Aktiengesellschaft	Stuttgart	D	TAR h 60/615/24VDC 3 kW, 230 V	702.10	702.10
Total (EUR)							76,793.81

References

- Komonsing, N.; Reyer, S.; Khuwijitjaru, P.; Mahayothee, B.; Müller, J. Drying Behavior and Curcuminoids Changes in Turmeric Slices during Drying under Simulated Solar Radiation as Influenced by Different Transparent Cover Materials. *Foods* **2022**, *11*, 696. [[CrossRef](#)] [[PubMed](#)]
- Ntwali, J.; Schock, S.; Romuli, S.; Chege, C.; Banadda, N.; Aseru, G.; Müller, J. Performance Evaluation of an Inflatable Solar Dryer for Maize and the Effect on Product Quality Compared with Direct Sun Drying. *Appl. Sci.* **2021**, *11*, 7074. [[CrossRef](#)]
- Heindl, A. *Praxisbuch Bandtrocknung*; Springer Vieweg: Heidelberg, Germany, 2016.
- Jain, D.; Pathare, P. Selection and Evaluation of Thin Layer Drying Models for Infrared Radiative and Convective Drying of Onion Slices. *Biosyst. Eng.* **2004**, *89*, 289–296. [[CrossRef](#)]
- Esmaili, M.; Sotudeh-Gharebagh, R.; Mousavi, M.A.; Rezazadeh, G. Influence of dipping on thin-layer drying characteristics of seedless grapes. *Biosyst. Eng.* **2007**, *98*, 411–421. [[CrossRef](#)]
- Ghnimi, T.; Hassini, L.; Bagane, M. Experimental study of water desorption isotherms and thin-layer convective drying kinetics of bay laurel leaves. *Heat Mass Transf.* **2016**, *52*, 2649–2659. [[CrossRef](#)]
- Lopez, A.; Iguaz, A.; Esnoz, A.; Virseda, P. Thin-layer drying behaviour of vegetable wastes from wholesale market. *Dry. Technol.* **2000**, *18*, 995–1006. [[CrossRef](#)]
- Sonmete, M.H.; Menges, H.O.; Ertekin, C.; Özcan, M.M. Mathematical modeling of thin layer drying of carrot slices by forced convection. *J. Food Meas. Charact.* **2016**, *11*, 629–638. [[CrossRef](#)]
- Xanthopoulos, G.; Lambrinos, G.; Manolopoulou, H. Evaluation of Thin-Layer Models for Mushroom (*Agaricus bisporus*) Drying. *Dry. Technol.* **2007**, *25*, 1471–1481. [[CrossRef](#)]
- Goyal, R.; Kingsly, A.; Manikantan, M.; Ilyas, S. Thin-layer Drying Kinetics of Raw Mango Slices. *Biosyst. Eng.* **2006**, *95*, 43–49. [[CrossRef](#)]
- Fang, S.; Wang, Z.; Hu, X. Hot air drying of whole fruit Chinese jujube (*Zizyphus jujuba* Miller): Thin-layer mathematical modelling. *Int. J. Food Sci. Technol.* **2009**, *44*, 1818–1824. [[CrossRef](#)]
- Ajibola, O. Thin-layer drying of melon seed. *J. Food Eng.* **1989**, *9*, 305–320. [[CrossRef](#)]
- Dotto, G.L.; Meili, L.; Tanabe, E.H.; Chielle, D.P.; Moreira, M.F.P. Evaluation of the mass transfer process on thin layer drying of papaya seeds from the perspective of diffusive models. *Heat Mass Transf.* **2017**, *54*, 463–471. [[CrossRef](#)]
- Mocelin, B.; Oliveira, D.L.; Chielle, D.P.; Tanabe, E.H.; Bertuol, D.A.; Schwaab, M.; Meili, L. Mathematical Modeling of Thin Layer Drying of Papaya Seeds in a Tunnel Dryer Using Particle Swarm Optimization Method. *Part. Sci. Technol.* **2014**, *32*, 123–130. [[CrossRef](#)]
- Bengtsson, P.; Sanati, M. Evaluation of hydrocarbon emissions from heart- and sapwood of Scots pine using a laboratory-scale wood drier. *Holzforschung* **2004**, *58*, 660–665. [[CrossRef](#)]
- Mirahmadi, S.F.; Norouzi, R. Influence of Thin Layer Drying on the Essential Oil Content and Composition of *Lavandula officinalis*. *J. Essent. Oil Bear. Plants* **2016**, *19*, 1537–1546. [[CrossRef](#)]
- Reyer, S.; Awiszus, S.; Meissner, K.; Müller, J. High precision laboratory dryer for thin layer and bulk drying with adjustable temperature, relative humidity and velocity of the drying air. *HardwareX* **2020**, *8*, e00133. [[CrossRef](#)] [[PubMed](#)]
- VDI. Measurement of Fluid Flow with Primary Devices. In *Orifice Plates and Nozzles for Special Applications*; VDI: Düsseldorf, Germany, 1991; p. 2041.

19. Duc, L.A.; Han, J.W.; Keum, D.H. Thin layer drying characteristics of rapeseed (*Brassica napus* L.). *J. Stored Prod. Res.* **2011**, *47*, 32–38. [[CrossRef](#)]
20. Doymaz, I.; Gorel, O.; Akgun, N. Drying Characteristics of the Solid By-product of Olive Oil Extraction. *Biosyst. Eng.* **2004**, *88*, 213–219. [[CrossRef](#)]